Melting of Nanostructured Drugs Embedded into a Polymeric Matrix

P. Bergese,[†] I. Colombo,*[,‡] D. Gervasoni,[‡] and Laura E. Depero[†]

INSTM and Structural Chemistry Laboratory, University of Brescia, via Branze, 38, 25123 Brescia, Italy, and Physical Pharmacy Laboratory, Eurand S.p.A., via Martin Luther King, 13, 20060, Pessano con Bornago, Milano, Italy

Received: March 19, 2004; In Final Form: July 28, 2004

The melting behavior of nanostructured organic materials (drugs) embedded into a cross-linked polymeric matrix was studied for the first time. The complex microstructure of these nanocomposites, yielded by the polymer matrix in which molecular clusters and nanocrystals of drug plus a cospiquous fraction of water are confined, demanded synergic application of thermal analysis and temperature resolved X-ray diffraction. A relevant depression of the melting point of the embedded drug with respect to the bulk drug was experimentally demonstrated. The coherent domain size of the embedded drug nanocrystals was independently evaluated by thermal and diffraction data and results were in agreement. This indicates that the adopted thermodynamic melting model, based on Laplace and Gibbs−Duhem equations and developed for simpler systems, can be successfully assessed for describing drug/polymer nanocomposites, and, potentially, other classes of organic nanocomposites.

Introduction

The oral route is considered the best way of dosing drugs.[1] Orally administrated drugs dissolve in the gastrointestinal tract and enter the systemic circulation by molecular diffusion through the tract epithelial cell layer. Drug dissolution is thus a key parameter for assessing bioavailability and onset of action of oral dosage forms.[2,3] For a given drug that dissolves into the gastrointestinal tract, the drug molecules and the environment are fix parameters, and drug dissolution can be tailored only by microstructure manipulation.[4] In particular, dissolution can be enhanced by forcing the crystalline drug to assume a nanodimensional periodicity,[5] which is intertwined with a dramatic increase of the interface boundaries and a change of the melting temperature[6] and enthalpy.[7] This approach allows one to make bioavailable poorly soluble drugs, which represent 40% of all drugs.[8] Therefore, thermodynamics of nanostructured drugs is of interest from both a fundamental and a technological standpoint. However, few studies exist on this subject,[9−13] and most of them are focused on the effects of crystal size[11] and disorder[12,13] on dissolution.

The melting temperature of both free-standing and matrix confined nanostructured materials deviate from the bulk value. Deviations are related to the curvature[6] and the nature[6,14−17] of the interfaces. The phenomenon has been investigated for metals,[15,16,18−26] semiconductors,[15,27−29] organic materials[17,30−33] (including drugs[9,10] and polymer crystals[34]), and water.[35] Furthermore, condensation of water in nanosized geometries is the working principle of thermoporometry.[36−39]

The shifting of the melting point in nanosized materials was yet predicted by the thermodynamic nucleation theory in the early 1900s (Gibbs−Thomson equation).[30,40] Afterward, this approach was reconsidered by more sophisticated treatments,[19,36] which were then adapted to different melting mechanisms[21,23,36] and the eventual presence of a matrix.[14,22,36] Size dependency of the melting temperature was also approached by molecular dynamics,[41] which provided further indications on the possible melting mechanisms.[16,33,42−44] The melting enthalpy displays a size dependency somehow analogous to that of the melting temperature,[23,30,32,36,42] but it has been less studied.[7]

Melting of nanosized materials was experimentally investigated, apart from thermal analysis, by temperature resolved electron[18,27] and X-ray diffraction (XRD),[21,26,35] transmission electron microscopy (TEM),[17,23] and Brillouin scattering.[24]

To date, several works on melting of organic nanocrystals confined into porous silica glasses have been published,[10,17,30−33] but melting of organic nanocrystals embedded into polymers has still not been investigated. In the present paper, covering this lack, the melting point depression of drug nanocrystals confined into a cross-linked polymer is experimentally demonstrated and discussed. These kind of nanocomposites find wide application in bioavailability enhancement of poorly water-soluble drugs.[8]

Owing to their complex microstructure, the nanocomposites were investigated by coupling differential scanning calorimetry (DSC) and temperature resolved XRD, which was already successfully applied to track phase transitions of drugs,[45,46] and implemented for quantitative analysis of drug/polymer composites.[47] The coherent domain size of the nanocrystals was independently evaluated by XRD profile analysis and from melting point depression data. Thermal data were manipulated through a thermodynamic model based on Laplace and Gibbs−Duhem equations.[23,36] The comparison of the results from the different approaches allowed to test the model reliability.

Materials and Methods

I. Materials and Experimental Procedures. Griseofulvin (an antibiotic, $C_{17}H_{17}ClO_6$), lot VP01054, was supplied by Welding GmbH & Co. (Germany). Nifedipine (an antianginal, $C_{17}H_{18}N_2O_6$), lot T-02013, was supplied by Moehs Catalana S.A. (Spain). The cross-linked polyvinylpirrolidone ([C_6H_9-

[†] University of Brescia.
[‡] Eurand S.p.A.
* Corresponding author. Telephone: +39 0295428 ext. 458. Fax: +39 0295745012. E-mail: icolombo@eurand.it.

10.1021/jp048762u CCC: $27.50
Published on Web 09/14/2004

NO]$_n$), popular as crospovidone, Kollidon CL-M lot VP-00050, hereafter referred as PVPCLM, was obtained from BASF Italia S.p.A. (Italy). The raw materials were worked as received by a high energy mechanic activation (HEMA) patented process[48] that allows to generate nanocomposites made of PVPCLM microparticles in which nanocrystals and molecular clusters of drug are confined, and a nonnegligible fraction of water is absorbed.[48−51] The physical mixtures of raw drug and PVPCLM powders, in a weight ratio of 1/5 w/w, were cold co-grinded in a high energy vibration mill at 1400 rpm. The griseofulvin/PVPCLM mixture was worked for 1 h, while the nifedipine/PVPCLM one was worked for 2 h. Hereafter, the nanocomposites of griseofulvin/PVPCLM and of nifedipine/PVPCLM will be referred as N1 and N2, respectively.

Temperature resolved X-ray diffraction (XRD) experiments were performed on a Philips X′Pert PRO diffractometer (θ/θ Bragg−Brentano geometry) equipped with a variable temperature chamber (TTK 450 by Anton Paar GmbH). Cu Kα radiation (λ = 1.541 Å), generated by a sealed X-ray tube (45 kV × 40 mA), and a real time multiple strip detector (X'Celerator by Philips) were used for all the XRD experiments. The working temperature was measured and controlled by a platinum thermocouple mounted at the sample holder surface. The nanocomposites (in the form of powders), after gentle manual grinding, were frontally loaded in the sample holder. The samples were heated with a rate of 10 °C min^{-1} and the XRD patterns collected every 5 °C with a scanning speed of 0.0102 deg s^{-1}. During pattern collections the samples were maintained at constant temperature. All the temperature resolved XRD experiments were performed in inert atmosphere (N_2) in order to avoid oxidative decompositions.

Thermal analysis were carried out with a power-compensated differential scanning calorimeter Pyris-1 and a thermogravimetric analyzer Pyris-1, both by Perkin-Elmer. The samples to be analyzed by DSC were put into aluminum pans (6−7 mg of nanocomposite and about 2 mg of raw drug) and then scanned under a N_2 stream of 20 cm^3 min^{-1} at a rate of 10 or 0.5 °C min^{-1}. The thermal profiles at 10 °C min^{-1} were collected for qualitative analysis and melting temperatures measurements, while the ones at 0.5 °C min^{-1} were collected for determining melting enthalpy of the bulk drugs. Temperature calibration was made, at each scan rate, using Hg and In as standards. Thermogravimetric analysis (TGA) were performed on powder samples of 8−9 mg at a scanning rate of 10 °C min^{-1} and under a N_2 stream of 35 cm^3 min^{-1}. DSC and TGA experiments for quantitative purposes were performed by a single heating program while experiments for collecting qualitative profiles were performed by a heating-cooling-heating program (heating from 20 to 100 °C, cooling to 20 °C and heating above the bulk drug melting temperature).

II. Quantitative X-ray Diffraction. The evolution of the weight fraction of the crystalline drug contained in the nanocomposites was tracked by quantitative XRD. We adopted a single-line method which was specifically developed for largely amorphous composites.[47] All the experiments were performed by heating the samples from 25 °C to 10 °C above the bulk drug melting temperature. As confirmed by the TGA profiles reported in Figures 3 and 4, during heating the nanocomposite samples lose the absorbed water. Water loss changes the initial weight ratio between the phases as well as the sample X-ray absorption coefficient. These quantities participate to determine the scale factor which links the phase weight fraction to the intensity of the related diffraction peak. It follows that the scale factor varies with temperature and in turn that the evolution with temperature of the intensity of a peak does not directly represent the evolution of the weight fraction of the related phase.

To take this effect into account we start by considering the general equation which relates the integrated intensity, I_{ij}, of the ith diffraction peak of the phase j to the weight fraction of this phase,[52] c_j

$$I_{ij} = K_e K_{ij} c_j / \rho_j \mu^* \tag{1}$$

where K_e is a constant for a particular experimental system, K_{ij} is a constant for each diffraction peak i from the phase j, ρ_j is the density of the phase j, and μ^* is the mass absorption coefficient of the sample. Equation 1 holds for randomly oriented powder samples measured in a Bragg−Brentano geometry.

μ^* is independent from the physical state and microstructure of the sample, since it is the weighted sum of the mass absorption coefficients of the single atoms. Consequently, at ambient temperature, T_A, the mass absorption coefficient of a drug/PVPCLM nanocomposite, μ^{*T_A}, reads

$$\mu^{*T_A} = \varphi_D \mu_D^* + \varphi_P \mu_P^* + \varphi_W \mu_W^* \tag{2}$$

where φ_D is the total (amorphous plus crystalline) drug weight fraction, φ_P is the PVPCLM weight fraction, and φ_W is the water weight fraction; μ_D^*, μ_P^*, and μ_W^* are the mass absorption coefficients of drug, PVPCLM, and water, respectively. By dividing factor by factor eq 1 written at T_A with the same equation written for a different experimental temperature, T_E, one obtains

$$I_{ij}^{T_A}/I_{ij}^{T_E} = \frac{K_e^{T_A} K_{ij}^{T_A} c_j^{T_A}}{\rho_j^{T_A} \mu^{*T_A}} \frac{\rho_j^{T_E} \mu^{*T_E}}{K_e^{T_E} K_{ij}^{T_E} c_j^{T_E}} \tag{3}$$

For drug/PVPCLM nanocomposites at a T_E varying between T_A and the drug melting temperature, T_m, it can be assumed that $\rho_D^{T_E} \cong \rho_D^{T_A}$, $K_e^{T_E} \cong K_e^{T_A}$, and $K_{iD}^{T_E} \cong K_{iD}^{T_A}$ (the suffix D stays for "drug crystalline phase"). Moreover, if at T_E all the water phase has been lost by the sample, then μ^{*T_E} may be written as $\mu^{*T_A} - \varphi_W \mu^*_W$. By using these observations, eq 3 can be rearranged in a working equation that links the weight fractions of the phase j at temperatures T_A and T_E with the relative diffraction intensities:

$$c_D^{T_E} = c_D^{T_A} (I_{iD}^{T_E}/I_{iD}^{T_A})(1 - \varphi_W \mu^*_W/\mu^{*T_A}) \tag{4}$$

Operatively, $c_D^{T_A}$, was determined by the method described in ref 47, and then $c_D^{T_E}$, calculated by eq 4. To assess the measurement precision, all the quantitative XRD experiments were repeated three times and the standard deviations (SDs) calculated.

III. (Thermodynamic) Melting Model. In drug/PVPCLM nanocomposites drug is embedded into the polymer according to two main arrangements: amorphous drug dispersed into the molecular cross-linked network of the polymer, and discontinuous layers of drug nanocrystals segregated onto the popcorn-like surface of the polymer. Nanocrystals are highly disordered and are aggregates of crystallites (or coherent domains) separated by amorphous boundaries. In molecular amorphous solids of low molecular weight, like drugs, the glass transition temperature, T_g, is primarily associated with melting. A solid drug at temperatures higher than T_g has a high molecular mobility; i.e., it is a supercooled liquid.[53−55] It follows that the amorphous boundaries melt before the drug crystallites, which in turn melt

surrounded by a drug liquid phase. Accordingly, we decided to describe the melting of the crystallites by the model developed by Brun et al.,[36] which is based on Laplace and Gibbs−Duhem equations. The model predicts that the melting temperature, T_m, of spherical crystallites separated from the gas phase by the liquid-phase satisfies the equation

$$T_m^{bulk} - T_m = \frac{2T_m^{bulk}}{h_m^{bulk}}\left[\upsilon_s\frac{\gamma_{sl}}{r_{sl}} + (\upsilon_s - \upsilon_l)\frac{\gamma_{lg}}{r_{lg}}\right] \quad (5)$$

where T_m^{bulk}, h_m^{bulk} are the bulk melting temperature and the bulk specific enthalpy of fusion, υ_s and υ_l are the specific volumes of the solid phase and of the liquid phase, r_{sl} and r_{lg} are the curvature radii of the solid−liquid interface (i.e., the crystallite radius) and of the liquid−gas interface, and γ_{sl} and γ_{lg} are the solid−liquid interfacial energy (per unit area) and the liquid−gas interfacial energy (per unit area).

To simplify eq 5, two situations can be considered. If the drug crystallites are dominant with respect to the amorphous boundaries, then they are tightly packed. In this case we can assume that melting starts with each crystallite covered by a liquid skin, which means that $r_{lg} \approx r_{sl}$. Therefore eq 5 reads as follows:

$$T_m^{bulk} - T_m = \frac{2T_m^{bulk}}{h_m^{bulk} r_{sl}}[\upsilon_s\gamma_{sl} + (\upsilon_s - \upsilon_l)\gamma_{lg}] \quad (6)$$

On the contrary, if the amorphous drug fraction is much larger than the crystalline one, then the crystallites melt dispersed in a liquid bath, and $r_{lg} \approx \infty$. In this case eq 5 becomes

$$T_m^{bulk} - T_m = \frac{2T_m^{bulk}\upsilon_s\gamma_{sl}}{h_m^{bulk} r_{sl}} \quad (7)$$

It might be noted that eqs 6 and 7 are two of the most popular equilibrium thermodynamic melting models. Equation 6 is the liquid shell model (LSM) when the liquid skin is much smaller than the crystallite radius, and eq 7 is the upper limit of the liquid nucleation and growth model (LNG).[23]

Equations 6 and 7 were used to evaluate the crystallites diameter, $D_T = 2r_{sl}$, from the experimental melting point depression, $\Delta T = T_m^{bulk} - T_m$. Being developed in the framework of equilibrium thermodynamics, these equations can be applied only to experimental data collected in quasi-equilibrium conditions. Therefore, the DSC profiles of the bulk drug used for the experimental determination of h_m^{bulk} (and T_m^{bulk}) were collected at 0.5 °C min^{-1}, at which the quasi-equilibrium approximation holds.[36−39]

The nanocomposites could not be scanned at 0.5 °C min^{-1} because of the very poor heat flow signal (in power compensated DSC the signal intensity is a function of the heating rate[56,57]). Consequently, to enhance the signal, the nanocomposites were scanned at 10 °C min^{-1} and T_m was determined. T_m also depends on the heating rate but this dependence was ruled out by the proper calibration procedure of the calorimeter, and thus the measured T_m could be used in the equilibrium eqs 6 and 7.

To assess their precision, the measurements were repeated three times and the standard deviations (SDs) calculated.

Results and Discussion

The XRD patterns at ambient temperature of bulk (raw) griseofulvin and of the griseofulvin/PVPCLM nanocomposite, N1, are shown in Figure 1. The XRD patterns of bulk (raw) nifedipine and of the nifedipine/PVPCLM nanocomposite, N2, are shown in Figure 2. In both figures, the matching of the Bragg peaks demonstrates that the crystallographic phase of the drug embedded into the polymeric matrix coincide with the raw drug phase.

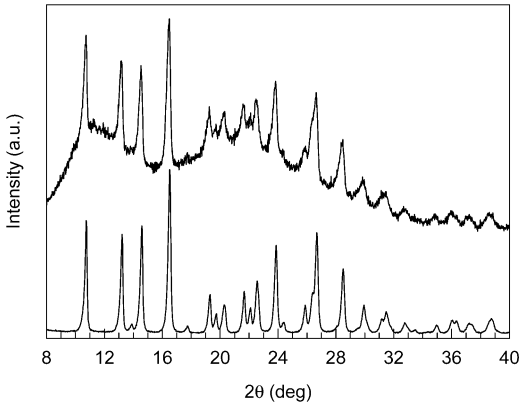

Figure 1. XRD pattern at ambient temperature of bulk griseofulvin (bottom) and of the nanocomposite N1 (top). The patterns have been scaled.

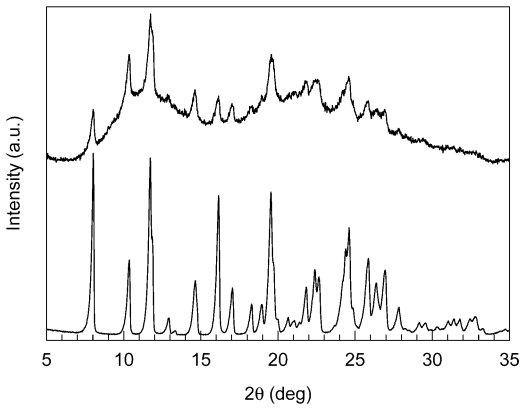

Figure 2. XRD pattern at ambient temperature of bulk nifedipine (bottom) and of the nanocomposite N2 (top). The patterns have been scaled.

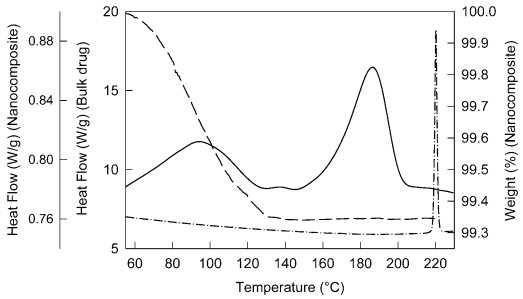

Figure 3. DSC profiles of bulk griseofulvin (dash−dotted line and left ordinate axis) and of N1 (continuous line and left ordinate offset axis), and TGA profile of N1 (dashed line and right ordinate axis).

Thermal analysis of N1 and bulk griseofulvin are reported in Figure 3. The DSC profile of N1 (continuous line) evidences two distinct endothermic events. Between 60 °C and 120 °C, in correspondence of the first event, the TGA (dashed line) register a weight loss, indicating that the event is related to the loss of the water absorbed into the PVPCLM matrix. The second event can then be ascribed to the melting of the embedded crystalline griseofulvin. It follows that the melting temperature of the embedded griseofulvin, which is 187.8 ± 0.3 °C, is significantly lower than the melting temperature of the stand-alone bulk griseofulvin, which instead is 220.9 ± 0.1 °C, as

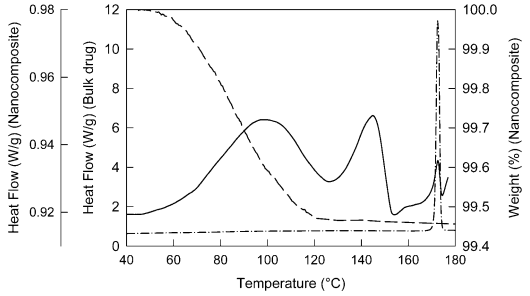

Figure 4. DSC profiles of bulk nifedipine (dash−dotted line and left ordinate axis) and of N2 (continuous line and left ordinate offset axis), and TGA profile of N2 (dashed line and right ordinate axis).

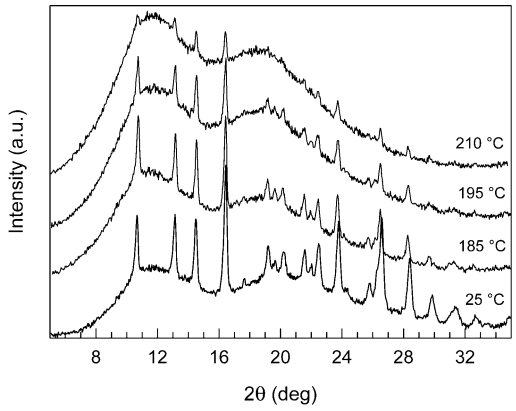

Figure 5. Representative XRD patterns of N1 at different temperatures.

shown by its DSC profile (dash−dotted line). This result was expected because the griseofulvin embedded into PVPCLM is nanostructured,[48] and it is in agreement with previous observations.[9] According to the melting models, crystals with different sizes melt at different temperatures, and thus the melting peak profile is determined by the crystal size distribution. Since this effect is significant only at the nanoscale and shades at the macroscopic scale, the melting peak of a nanocrystalline material is expected to be significantly broadened with respect to the one of the bulk material. This feature, already observed[9,23,30] in other materials, can be observed also by comparing N1 and bulk griseofulvin DSC profiles.

In Figure 4 the DSC profiles of N2 (continuous line) and of bulk nifedipine (dash−dotted line) are reported. The N2 profile shows three main features: the first endothermic event related to the water loss and two endothermic peaks. The second peak is centered at the melting temperature of bulk nifedipine, which is 172.5 ± 0.2 °C. The peak is then related to the melting of the bulk fraction of nifedipine contained in N2 which crystallized out of the polymer matrix. Then, considerations analogous to those given for N1 indicate that the first peak, centered at 142.9 ± 0.2 °C, is determined by the melting of the nanocrystalline nifedipine fraction.

Temperature resolved XRD was used to gain a deeper insight into the melting of the embedded drug. In Figures 5 and 6 representative patterns of N1 and N2 at ambient temperature and at temperatures below the melting temperature of the bulk drug are shown. Except for the intensities, the high temperature patterns match the pattern at ambient temperature. This allowed us to point out that the only drug phase transformation occurring during heating was melting and to chose the Bragg peaks more suitable for quantitative single-line analysis.

We selected the peak at $2\theta = 10.70°$ for N1 and the one at $2\theta = 11.76°$ for N2, because they exhibited satisfactory intensities and could be easily corrected for the background.

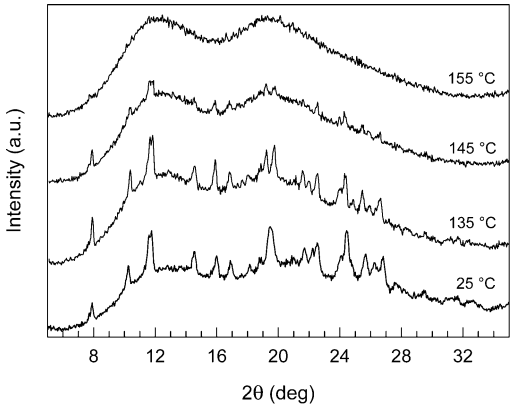

Figure 6. Representative XRD patterns of N2 at different temperatures.

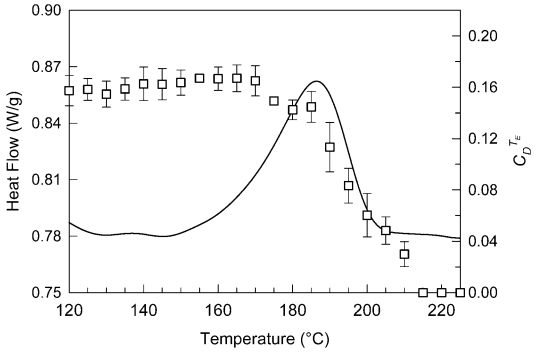

Figure 7. DSC profile of N1 (continuous line and left ordinate axis) and weight fraction ($c_D^{T_E}$) of crystalline griseofulvin embedded into N1 (open squares and right ordinate axis). Standard deviations are indicated by the error bars.

Consequently, the N1 patterns for quantitative XRD were collected from $2\theta = 9.50°$ to $2\theta = 11.50°$, and the N2 patterns from $2\theta = 10.80°$ and $2\theta = 12.80°$. The temperature ranges for the XRD experiments were selected on the basis of thermal data: N1 was studied from 25 to 225 °C, while N2 was studied from 25 to 180 °C. N1 was measured to have a total drug content, φ_D, equal to 0.167, a weight fraction of crystalline drug at ambient temperature, $c_D^{T_A}$, equal to 0.133 ± 0.008 and a weight fraction of absorbed water, φ_W, equal to 0.060 ± 0.003. The values for N2 were: $\varphi_D = 0.164$, $c_D^{T_A} = 0.134 \pm 0.004$, and $\varphi_W = 0.107 \pm 0.004$. The mass absorption coefficients for Cu Kα radiation, μ^{*T_A}, were calculated to be 7.137 and 5.676 $cm^2\ g^{-1}$ for N1 and N2, respectively.

The evolution with temperature of $c_D^{T_E}$ in N1 and N2 is reported by the open squares in Figures 7 and 8 respectively, the measurement SDs are indicated by the error bars. To make easier the comparison between thermal and diffraction data, in the figures the $c_D^{T_E}$ plot is superimposed to the DSC profile. Figure 7 shows that in N1, $c_D^{T_E}$ decreases to 0 in correspondence to the endothermic event centered at $T_m = 187.8$ °C. This unambiguously confirms that the thermal event is the melting of the embedded crystalline griseofulvin, and thus that it melts at a lower temperature than bulk griseofulvin. A similar behavior is displayed by the crystalline nifedipine embedded in N2. As shown in Figure 8, $c_D^{T_E}$ decreases in correspondence of the first endothermic curve, centered at 142.9 °C, and becomes zero before the second melting curve, occurring at 172.5 °C, which is related to the melting of the bulk nifedipine contained in N2 (see also Figure 4). Again, this indicates that the melting point of the embedded drug is significantly depressed with respect to the bulk drug. The bulk drug contained in N2 was not detected by XRD. This is due to the fact that its weight fraction

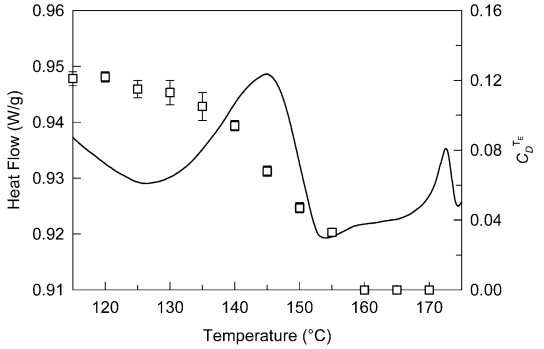

Figure 8. DSC profile of N2 (continuous line and left ordinate axis) and weight fraction ($c_D^{T_E}$) of crystalline nifedipine embedded into N2 (open squares and right ordinate axis). Standard deviations are indicated by the error bars.

(estimated by DSC quantitative analysis[58] to be 0.017) results below the detection limit of the XRD experiment.

Crystallite sizes and microstrains of the embedded drug were evaluated from the XRD profiles by applying the double-Voight analysis method.[59] The instrumental profile was analyzed by the fundamental parameters approach (FPA),[60] and the profile fitting was performed by the software TOPAS P.[61] The analyzed Bragg peaks for griseofulvin (N1) were those at $2\theta = 10.70°$, $2\theta = 13.15°$, $2\theta = 14.51°$, and $2\theta = 16.43°$, while for nifedipine (N2) Bragg peaks were those at $2\theta = 8.00°$, $2\theta = 10.33°$, and $2\theta = 14.60°$. The statistical quality index R_{wp} was always lower than 3.5%.

For any analyzed peak, the double-Voight method allows to calculate the volume-weighted height of the crystallites, ϵ_β, along the crystallographic direction [*hkl*] represented by the peak. The volume-weighted average height (i.e., diameter) of the crystallites, $\langle D_V \rangle$, can be obtained by averaging the ϵ_β values given by each peak. Nanostructured griseofulvin resulted to be composed by crystallites of $\langle D_V \rangle = 26 \pm 1$ nm, and nifedipine by crystallites of $\langle D_V \rangle = 21 \pm 1$ nm. For the embedded drugs, microstrain indicates the intercrystallite disorder,[62] and it was calculated to be 0.08 ± 0.02 and 0.04 ± 0.02 for griseofulvin and nifedipine, respectively. Such orders of magnitude and higher are common in HEMA worked materials.[63]

The crystallite diameter was also evaluated from the melting data by the thermodynamic models presented in the Materials and Methods section. The thermodynamic quantities required by the models were experimentally determined for both the drugs. The melting point depression of the embedded griseofulvin, ΔT, and the bulk griseofulvin specific enthalpy of fusion, h_m^{bulk}, were obtained by DSC analysis and resulted in 33.1 ± 0.3 °C and 110.6 ± 1.0 J g^{-1} respectively. The specific volumes of solid and liquid griseofulvin, v_s and v_l, were measured by helium picnometry and calculated using the group contribution method.[64] The obtained values were 6.69×10^{-7} and 7.23×10^{-7} m^3 g^{-1} respectively. The solid−gas, the liquid−gas, and the solid−liquid interfacial energies, γ_{sg}, γ_{lg}, and γ_{sl}, were evaluated by contact angle experiments[65] and the parachor method.[66] The calculated values were $\gamma_{sg} = 6.22 \times 10^{-2}$ J m^{-2}, $\gamma_{lg} = 5.25 \times 10^{-2}$ J m^{-2}, and $\gamma_{sl} = 3.47 \times 10^{-2}$ J m^{-2}. The equivalent data for nifedipine were as follows: $\Delta T = 29.6 \pm 0.3$ °C, $h_m^{bulk} = 107.5 \pm 0.7$ J g^{-1}, $v_s = 7.27 \times 10^{-7}$ m^3 g^{-1}, $v_l = 7.86 \times 10^{-7}$ m^3 g^{-1}, $\gamma_{sg} = 5.25 \times 10^{-2}$ J m^{-2}, $\gamma_{lg} = 4.61 \times 10^{-2}$ J m^{-2}, and $\gamma_{sl} = 2.21 \times 10^{-2}$ J m^{-2}.

By using the above data the LSM model gave a diameter, D_T, equal to 11.0 ± 0.1 and 7.5 ± 0.1 nm for griseofulvin and nifedipine, respectively. Instead, the LNG model gave 12.5 ± 0.1 and 9.0 ± 0.1 nm for griseofulvin and nifedipine, respectively. The difference between the results from the two opposite approximations is very small and close to the measurement uncertainties, and the real D_T of the crystallites should lie between them. However, according to quantitative XRD, the 79.6% of the griseofulvin embedded in N1, and the 81.7% of the nifedipine embedded in N2 are crystalline phases of the drugs. Therefore, the embedded nanocrystals are probably made of crystallites separated by thin amorphous boundaries, and the LSM model is more appropriate to describe their melting.

For both drugs, the mean crystallite diameter estimated by XRD, $\langle D_V \rangle$, is about 2.5 times higher than the one obtained by the thermodynamic model, D_T. This difference is due to the fact that $\langle D_V \rangle$ is the volume-weighted mean diameter of the crystallites and D_T is the most probable value (mode) of the volumetric distribution of the crystallite diameters (obtained from melting enthalpy). In general, the crystallite diameter distribution is a log-normal function,[67,68] and thus its mode is lower than its weighted mean.

At the light of the above considerations, the results are in fairly good agreement. It follows that the melting thermal data are properly linked to the size of the crystallites by the classic thermodynamic model described in the Materials and Methods section.

Conclusions

The melting behavior of nanostructured griseofulvin and nifedipine embedded into PVPCLM was studied by combining thermal analysis and temperature resolved XRD. A relevant depression of the melting point with respect to the bulk drug was found for griseofulvin ($\Delta T = 33.1$ °C) as well as for nimesulide ($\Delta T = 29.6$ °C). The coherent domain (crystallite) size of the embedded drugs was independently evaluated by both thermal and diffraction data, and the results were consistent. The more probable dimension of the coherent domains distribution was estimated to be 11.0 and 7.5 nm for griseofulvin and nifedipine, respectively.

The results confirmed that the depression of the melting point of the embedded drugs is linked to their packing in nanosized coherent domains. The good agreement between the size results obtained from XRD and thermal data suggests that, for sizes around 10 nm, the assumed equilibrium thermodinamics melting model, based on the Laplace and the Gibbs−Duhem equations, well describes the correlation between the crystallite size and the melting point shift of the embedded drug. Therefore, this classic approach, which was developed and used for simpler systems, such as isolated nanoparticles, nanostructured thin films, and materials confined into monodispersed nanoporous silica glasses, can be successfully adapted to drug/crospovidone nanocomposites and, potentially, to other class of nanostructured organic materials embedded into polymer matrixes.

References and Notes

(1) Devane, J. *Pharm. Technol.* **1998**, *Nov.*, 68.

(2) *Waiver of in vivo bioavailability and bioequivalence studies for immaediate-release solid oral dosage forms based on a biopharmacutics classification system*; U.S. Department of Health and Human Services, Food and Drug Administration, Center for Drug Evaluation and Research: Washington, DC, 2000. Also available at: http://www.fda.gov/cder/guidance/index.htm.

(3) Amidon, G. L.; Lennearnas, H.; Shah, V. P.; Crison, R. *Pharm. Res.* **1995**, *12*, 413.

(4) Hsia, D. C.; Kim, C. K.; Kildsig, D. O. *J. Pharm. Sci.* **1977**, *66*, 961.

(5) Bergese, P. Ph.D. Thesis, Pharmaceutical nanocomposites generated by microwave induced diffusion. Università degli studi di Brescia: Brescia, Italy, 2002; pp 12−19.

(6) Zhao, M.; Zhou, X. H.; Jiang, Q. *J. Mater. Res.* **2001**, *16*, 3304.

(7) Liang, L. H.; Zhao, M.; Jiang, Q. *J. Mater. Sci. Lett* **2002**, *21*, 1843.
(8) Liu, R., Ed. *Water-Insoluble Drug Formulation*; Interpharm Press: Denver, CO, 2000.
(9) Carli, F.; Colombo, I.; Magarotto, L. In *13th International Symposium on controlled release of bioactive materials*; Nortfolk, Chaudy, I., Ed.; The Controlled Release Society: Minneapolis, MN, 1986; p 193.
(10) Carli, F.; Colombo, I. *Acta Pharm. Jugosl.* **1988**, *38*, 361.
(11) Bukton, G.; Beezer, A. E. *Int. J. Pharm.* **1992**, *82*, R7.
(12) Mosharraf, M.; Sebhatu, T.; Nystrom, C. *Int. J. Pharm.* **1999**, *177*, 29.
(13) Burt, H. M.; Mitchell, A. G. *Int. J. Pharm.* **1981**, *9*, 137.
(14) Allen, G. L.; Gile, W. W.; Jesser, W. A. *Acta Metall.* **1980**, *28*, 1695.
(15) Shi, F. G. *J. Mater. Res.* **1994**, *9*, 1307.
(16) Lu, K.; Jin, Z. H. *Curr. Opin. Solid State. Mater.* **2001**, *5*, 39.
(17) Sanz, N.; Boudet, A.; Ibanez, A. *J. Nanop. Res.* **2002**, *4*, 99.
(18) Takagi, M. *J. Phys. Soc. Jpn.* **1954**, *9*, 359.
(19) Couchman, P. R.; Jesser, W. A. *Nature (London)* **1977**, *269*, 481.
(20) Lu, K.; Sui, M. L. *Acta Metall. Mater.* **1995**, *43*, 3325.
(21) Peters, K. F.; Cohen, J. B.; Chung, Y. W. *Phys. Rev. B* **1998**, *57*, 13430.
(22) Sheng, H. W.; Lu, K.; Ma, E. *Acta Mater.* **1998**, *46*, 5195.
(23) Zhang, M.; Efremov, M. Y.; Schiettekatte, F.; Olson, E. A.; Kwan, A. T.; Lai, S. L.; Wisleder, T.; Greene, J. E.; Allen, L. H. *Phys. Rev. B* **2000**, *62*, 10548.
(24) Bottani, C. E.; Li Bassi, A.; Stella, A.; Cheyssac, P.; Kofman, R. *Europhys. Lett.* **2001**, *56*, 386.
(25) Liang, L. H.; Li, J. C.; Jiang, Q. *Physica B* **2003**, *334*, 49.
(26) Depero, L. E.; Bontempi, E.; Sangaletti, L.; Pagliara, S. *J. Chem. Phys.* **2003**, *118*, 1400.
(27) Goldstain, A. N.; Echer, C. M.; Alivisatos, A. P. *Science* **1992**, *256*, 1425.
(28) Zhang, Z.; Zhao, M.; Jiang, Q. *Semicond. Sci. Technol.* **2001**, *16*, L33.
(29) Liang, L. H.; Li, J. C.; Jiang, Q. *Phys. Status Solidi B* **2003**, *236*, 583.
(30) Jackson, C. L.; McKenna, G. B. *J. Chem. Phys.* **1990**, *93*, 9002.
(31) Zhang, J.; Liu, G.; Jonas, J. *J. Phys. Chem.* **1992**, *96*, 3478.
(32) Jiang, Q.; Shi, H. X.; Zhao, M. *J. Chem. Phys.* **1999**, *111*, 2176.
(33) Sliwinska-Bartkowiak, M.; Dudziak, G.; Sikorski, R.; Gras, R. *J. Chem. Phys.* **2001**, *114*, 950.
(34) Rottele, A.; Thurn-Albrecht, T.; Sommer, J. U.; Reiter, G. *Macromolecules* **2003**, *36*, 1257.
(35) Handa, Y. P.; Zakrzewski, M.; Fairbridge, C. *J. Phys. Chem.* **1992**, *96*, 8594.
(36) Brun, M.; Lallemand, A.; Quinson, J. F.; Eyraud, C. *J. Chim. Phys.* **1973**, *70*, 979.
(37) Brun, M.; Lallemand, A.; Quinson, J. F.; Eyraud, C. *Thermochim. Acta* **1977**, *21*, 59.
(38) Homshaw, L. G. *J. Colloid Interface Sci.* **1981**, *84*, 141.
(39) Ishikiriyama, K.; Todoki, M.; Min, K. H.; Yonemori, S.; Noshiro, M. *J. Therm. Anal.* **1996**, *46*, 1177.
(40) Adamson, A. W.; Gast, A. P. *Physical Chemistry of Surfaces*; Wiley: New York, 2000.
(41) Bertsch, G. *Science* **1997**, *277*, 1619.
(42) Zhao, S. J.; Wang, S. Q.; Cheng, D. Y.; Ye, H. Q. *J. Phys. Chem. B* **2001**, *105*, 12857.
(43) Cheng, H. P.; Berry, R. S. *Phys. Rev. A* **1992**, *45*, 7969.
(44) Huang, S. P.; Balbuena, P. B. *J. Phys. Chem. B* **2002**, *106*, 7225.
(45) Rastogi, S.; Zakrzewski, M.; Suryanarayanan, R. *Pharm. Res.* **2001**, *18*, 267.
(46) Rastogi, S.; Zakrzewski, M.; Suryanarayanan, R. *Pharm. Res.* **2002**, *19*, 1265.
(47) Bergese, P.; Colombo, I.; Gervasoni, D.; Depero, L. E. *J. Appl. Crystallogr.* **2003**, *36*, 74.
(48) Lovrecich, M. Supported drugs with increased dissolution rate, and a process for their preparation. US Patent 5 449 521, 1995.
(49) Dobetti, L.; Cadelli, G.; Furlani, D.; Zotti, M.; Ceschia, D.; Grassi, M. *Proc. 28th Int. Symp. Contr. Relat. Bioact. Mater.* **2001**, 6059.
(50) Meriani, F.; Coceani, N.; Sirotti, C.; Voinovich, D.; Grassi, M. *J. Pharm. Sci.* **2004**, *93*, 540.
(51) Grassi, M. *Proc. AAPS Conf. Pharma. Drug Deliv.* **2004**.
(52) Alexander, L.; Klug, H. P. *Anal. Chem.* **1948**, *20*, 886.
(53) Yu, L. *Adv. Drug Del. Rew* **2001**, *48*, 27.
(54) Craig, D. Q. M.; Kett, V. L.; Murphy, J. R.; Price, D. M. *Pharm. Res.* **2001**, *18*, 1081.
(55) Boutonnet-Fagegaltier, N.; Menegotto, J.; Lamure, A.; Duplaa, H.; Caron, A.; Lacabanne, C.; Bauer, M. *J. Pharm. Sci.* **2002**, *91*, 1548.
(56) Saito, Y.; Saito, K.; Atake, T. *Themochim. Acta* **1986**, *107*, 279.
(57) Sauders, M.; Podluii, K.; Shergill, S.; Bukton, G.; Royall, P. *Int. J. Pharm.* **2004**, *274*, 35.
(58) Theeuwes, F.; Hussain, A.; Higuchi, T. J. *Pharm. Sci.* **1974**, *63*, 427.
(59) Balzar, D. In *Voight-function model in diffraction line-broadening ananlysis*; in *Defect and Microstructure analysis by diffraction*; Snyder, R. L., Bunge, H. J., Fiala, J.; Eds.; International Union of Crystallography, Oxford University Press: New York, 1999.
(60) Cheary, R. W.; Coelho, A. A. *J. Appl. Crystallogr.* **1992**, *25*, 109.
(61) Bruker AXS; *TOPAS V2.0: General profile and structure ananlysis software for powder diffraction data;* User manual, Bruker AXS: Karlsruhe, Germany, 2000.
(62) Enzo, S.; Fagherazzi, F.; Benedetti, A.; Polizzi, S. *J. Appl. Crystallogr.* **1988**, *21*, 536.
(63) Delogu, F.; Cocco, G. *J. Mater. Synth. Process.* **2000**, *8*, 271.
(64) Fedors, R. F. *Polym. Eng. Sci.* **1974**, *14*, 147.
(65) Wu, S. *J. Polym. Sci. C* **1971**, *34*, 19.
(66) Van Krevelen, D. W. *Properties of polymers*; Elsevier Science: Amsterdam, 1997.
(67) Langford, J. I.; Louer, D.; Scardi, P. *J. Appl. Crystallogr.* **2000**, *33*, 964.
(68) Balzar, D. *Report on the first size-strain round-robin of CPD*; IUCr; http://www.boulder.nist.gov/div853/balzar/s−s_rr.htm.